Effect of Vanadium Substitution on the Ni-Site in P2-Type $Na_{0.67}Ni_{0.33}Mn_{0.67}O_2$ in Optimized Carbonate Ester Electrolytes as Cathode for Sodium-Ion Batteries

Debanjana Pahari, Sreeraj Puravankara*

School of Energy Science and Engineering, Indian Institute of Technology Kharagpur, India – 721302

debanjana.pahari@iitkgp.ac.in, sreeraj@iitkgp.ac.in

Abstract

Solid-state synthesis of novel electrode materials of P2-type layered oxides $Na_{0.67}Ni_{0.33-x}V_xMn_{0.67}O_2$ (where, x = 0, 0.05, and 0.11) for the application as cathode materials in rechargeable non-aqueous sodium-ion batteries is reported. $Na_{0.67}Ni_{0.22}V_{0.11}Mn_{0.67}O_2$ electrode delivers significantly improved capacity retention than the pristine P2-$Na_{0.67}Ni_{0.33}Mn_{0.67}O_2$ when cycled between 1.5 and 4.3 V. The effect of organic ester electrolytes with 1.0 M $NaClO_4$ shows diverse effects in the cathode material. The best capacity retention for V-substituted electrodes is observed in Ethylene carbonate (EC): Propylene carbonate (PC): Dimethyl carbonate (DMC) (0.45: 0.45: 0.1) with 1.0 M $NaClO_4$ salt at a C-rate of 0.2C among four different ester electrolytes investigated [PC, EC: PC (1: 1), EC: DEC (1: 1) and EC: PC: DMC (0.45: 0.45: 0.1)].

1. Introduction

Layered transition metal oxides as successful cathode materials for aprotic sodium-ion batteries have experienced great interest in the last decade [1, 2, 3, 4]. The traditional transition metal layered oxides involve edge-sharing octahedral TMO_6 layers as alternative sheets (TM = transition metal). Na-ions are packed within two TMO_6 layers to devise a general formula of Na_xTMO_2. The alternate stacking of Na-ion and TMO_6 layers results in flexibility in the crystal lattice structure. As a result, three major classes of compounds (i.e., P2-, P3- and O3-phases) can be identified arising from the site preferences of Na-ions and the number of TMO_6 oxide layers [5]. In an O3-type structure, mobile Na-ions hop from one octahedral site to the nextlayer's octahedral site via an interstitial tetrahedral site resulting in a high activation energy barrier. In contrast, the ionic conduction in the P2-type structure occurs via hopping through the rectangular faces of the trigonal prism, implying low activation energy to cross via tetrahedral-tetrahedral face. Therefore, low energy diffusion pathways in P2-type structures establish the most preferred choice for high-performance material compared to O3-type structures. Both phases of V-based layered oxide O3-$NaVO_2$ and P2-Na_xVO_2 have been investigated in the early 2010s [6, 7]. Both the phases exert a reversible capacity of ~ 125 $mAhg^{-1}$, leading to a Na-intercalation/de-intercalation of 0.5 moles between 1.2 and 2.4 V. However, the redox voltage does not fall in either of the cathode or anode range which makes the utility of such materials complicated in real battery applications [8, 9]. P2-$Na_{2/3}[Ni_{1/3}^{2+}Mn_{2/3}^{4+}]O_2$ as a high-performance cathode material showed an average operating voltage of 3.5 V with a $Ni^{2+/4+}$ redox reaction, delivering approximately 160 $mAhg^{-1}$ in a voltage range of 2–4.5 V. However, it fails to exert good cycle stabilities owing to irreversible structural transformation and Na-ion/vacancy ordering transitions. Previous studies report how to increase the reversible capacity/cycling stability of this material by partial substitution at the transition metal site, like monovalent element such as (Li^+) [10], divalent elements such as Magnesium (Mg^{2+}) [11], zinc (Zn^{2+}) [12] and Copper (Cu^{2+}) [13], trivalent elements such as Iron (Fe^{2+}) [14] and Cobalt (Co^{3+}) [15] and tetravalent element Titanium (Ti^{4+}) [16]. The reported aliovalent substitutions involve both the TM-sites, Ni^{2+} as well as Mn^{4+}-site. Co^{3+} dopant in the Ni-site as P2-$Na_xNi_{0.22}Co_{0.11}Mn_{0.66}O_2$ cathode manifests an initial capacity of 117 $mAhg^{-1}$ with an average voltage of 3.3 V vs. Na/Na^+ and remarkable capacity retention over 200 cycles [17]. However, P2-$Na_xNi_{2/3}Co_{1/6}Mn_{1/6}O_2$ (Co^{3+} dopant on Mn-site) has displayed high initial discharge capacities and potentials as 216 $mAhg^{-1}$, 2.87 V vs. Na/Na^+ [18]. Aliovalent substitution in the Ni-site certainly lowers the specific capacity due to reduced electrochemically active Ni^{2+} sites, but the gain is in the improved average voltage and capacity retention. In order to incorporate electrochemically active similar valence Cu^{2+} sites into the Ni^{2+}-sites air-stable P2-type $Na_{2/3}Ni_{1/3-x}Cu_xMn_{2/3}O_2$ ($0 \leq x \leq 1/3$) electrodes were investigated [19]. Additional capacity due to Cu^{2+}/Cu^{4+} redox, improved capacity retention, and controlled phase changes enhance the electrochemical performance. A recent study on suppressing P2-O2 structural transition by optimum Ti-substitution reveals that the substituted electrodes can minimize the reversible capacity loss up to 12% during 50 charge-discharge cycles [20]. Aliovalently substituted cathodes have been studied at a full-cell level in order to realize practical applications. For example, a full cell containing O3-type $Na[Ni_{1/3}Fe_{1/3}Mn_{1/3}]O_2$ (Fe^{2+} dopant in the Mn-site) as cathode and hard carbon as anode has

delivered a specific discharge capacity of 100 $mAhg^{-1}$ during 150 cycles between 2.0 and 4.0 V at a rate of 0.5C [21]. A hard-carbon//$Na_{2/3}Ni_{1/3}Mn_{1/2}Ti_{1/6}O_2$ full-cell delivered an energy density of 300 $Whkg^{-1}$ comparable to Li-ion battery systems (graphite//$LiMn_2O_4$) [22]. Pentavalent dopants such as V^{5+}-ion on the Ni-site of P2-type $Na_{0.67}Ni_{0.33}Mn_{0.67}O_2$ have not been investigated to date. The effectiveness of aliovalent substitutions motivated the present study to realize the effect upon V-doping in the Ni-site of $Na_{2/3}[Ni_{1/3}^{2+}Mn_{2/3}^{4+}]O_2$ as cathodes for the application in non-aqueous sodium-ion batteries.

The effect of various organic electrolytes (ester-based, ether-based), their combinations, and additives were reported in the literature [23-25]. The varying reduction potentials [26] and SEI layer composition [27] of these electrolytes lead to a significant change in the electrode performance of the cathodes. The first study on P2-$Na_{2/3}[Ni_{1/3}^{2+}Mn_{2/3}^{4+}]O_2$ cathodes was performed in the presence of 1 M $NaPF_6$ in 33% ethylene carbonate (EC) - 67% diethyl carbonate (DEC) electrolyte between 2.0 and 4.5 V [28]. Many electrolyte combinations have been tested later in P2-$Na_{2/3}[Ni_{1/3}^{2+}Mn_{2/3}^{4+}]O_2$/Na half-cells. Propylene carbonate (PC) based solvents are very popular due to their high voltage stability and ionic conductivity [29]. The addition of a 2% Fluoroethylene carbonate (FEC) additive in 1 M $NaClO_4$/PC can efficiently extend the electrochemical stability to 4.5 V vs. Na/Na^+. P2-$Na_{2/3}[Ni_{1/3}^{2+}Mn_{2/3}^{4+}]O_2$ electrodes can exhibit a specific discharge capacity of 164 $mAhg^{-1}$ in the presence of the above electrolyte combination [30]. The most typical electrolyte combination in P2-$Na_{2/3}[Ni_{1/3}^{2+}Mn_{2/3}^{4+}]O_2$ based systems is 1 M $NaClO_4$/PC-FEC (95:5) [31, 32]. Moreover, comprehensive research reveals that the addition of 10% dimethyl carbonate (DMC) in the ethylene carbonate (EC) - propylene carbonate (PC) matrix eventually leads to improved ionic conductivity and low viscosity [33]. Therefore, in this article, we also aim to understand the effects of few other accepted binary/ternary electrolyte systems, including ethylene carbonate (EC) - propylene carbonate (PC), ethylene carbonate (EC) - diethyl carbonate (DEC), and ethylene carbonate (EC) - propylene carbonate (PC) - dimethyl carbonate (DMC) with 1 M $NaClO_4$ as the electrolytic salt.

2. Experimental Section

2.1. Synthesis of materials

Stoichiometric amounts of Mn_2O_3 (Manganese (III) oxide 99.9% trace metals basis, Sigma Aldrich), NiO (Nickel Oxide Green 75% (Ni) Extra Pure, Loba Chemie), and an excess of Na_2CO_3 (Sodium Carbonate Anhydrous 99.5% Extra Pure, Loba Chemie) powders were ground and mixed, then pellets (2 cm diameter and 1 cm high) were pressed. A solid-state reaction was then performed in air at 900^0C for 24 hours. The pellets were reground, pelletized, and the annealing was repeated. The sintered pellets were then quenched directly into liquid N_2. The Aliovalent atom (V^{5+}) doped samples of $Na_{0.67}Ni_{0.33-x}V_xMn_{0.67}O_2$ were prepared according to their stoichiometric ratio (x= 0.05 and 0.11) by using V_2O_5 as a precursor material.

2.2. Material characterization

All the powder samples were characterized using powder X-ray diffraction, and data were collected using Bruker D2-PHASER diffractometer (Cu Kα radiation, λ = 1.540598 Å) with

scanning from 10 to 80^0 two-theta region. The EPR spectra were collected from Bruker ELEXSYS 580 EPR spectrometer as a first derivative of the absorption signal in the X-band (9.6GHz) at room temperature.

2.3. Electrochemical characterization

Electrochemical tests were carried out using Na metal disc as the counter electrode and 1.0 M $NaClO_4$/Ethylene carbonate (EC) + Diethyl carbonate (DEC) (1:1, v/v) as electrolyte. 1.0 M $NaClO_4$ in Ethylene carbonate: Propylene carbonate: Dimethyl carbonate (0.45:0.45:0.1), 1.0 M $NaClO_4$ in Ethylene carbonate: Diethyl carbonate (1:1), 1.0 M $NaClO_4$ in Ethylene carbonate: Propylene carbonate (1: 1) and 1.0 M $NaClO_4$ in Propylene carbonate electrolytes were also employed to understand the electrode properties at various electrolytic conditions. A glass fiber filter (Whatman GF/C) was used as a separator. The electrode was composed of 70 wt. % active material, 20 wt.% Acetylene black and 10 wt.% PVDF binder. Electrode mixture was dispersed into N-methyl pyrrolidone (NMP), deposited onto metallic Al-foil, and dried at 80^0C under vacuum. Electrochemical performances of the cell were evaluated using an electrochemical workstation (BioLogic Instruments BCS-810) within the voltage range of 1.5-4.1 and 1.5-4.3 V.

3. Results and Discussion

3.1. Material characterization

3.1.1. Powder X-ray diffraction

The presence of the P2-type unit cell was confirmed through X-ray diffraction for all the synthesized samples. Fig.1 shows the diffraction patterns of all the P2-type layered structures of the solid solutions of V-substituted materials with general formula $Na_{0.67}Ni_{0.33-x}V_xMn_{0.67}O_2$ (where, x = 0, 0.05, and 0.11). The diffraction patterns are found to be iso-structural with the theoretically generated pattern (PDF-00-054-0894). The peaks can be indexed to the reported prismatic structure type with space group $P6_3/mmc$. No appearance/disappearance of diffraction peaks confirm the retention of long-range ordered structures of the pristine material even with V-substitution. A slight shift of the most intense (002) peak to higher angles has been observed upon V-substitution. The replacement of larger size Ni^{2+}-ions (ionic radii 0.69Å) by smaller size V^{5+}-ions (ionic radii 0.54Å) creates lattice shrinkage, successively reducing the interlayer oxygen atom repulsion. The right shift of the (002) peak and the observed reduced peak intensity are shown in the inset of Fig.1.

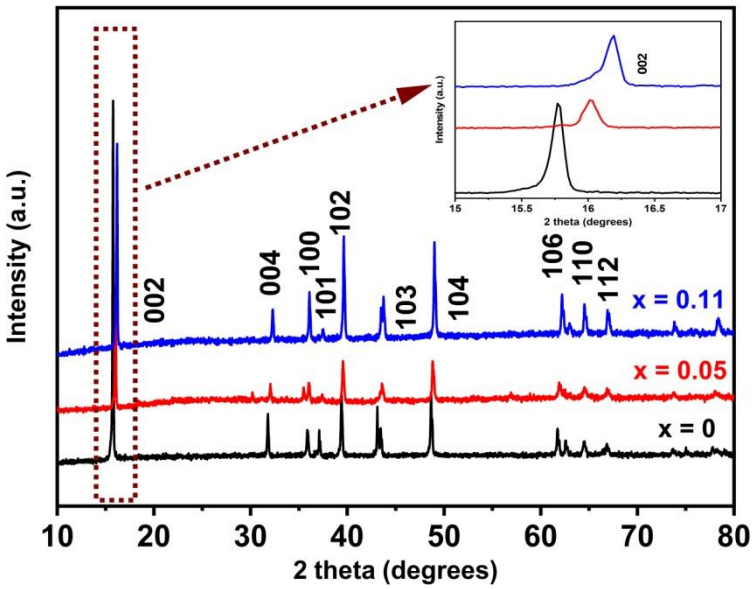

Fig.1: X-ray diffraction patterns of P2-$Na_{0.67}Ni_{0.33-x}V_xMn_{0.67}O_2$ (x= 0, 0.05 and 0.11) samples.

3.1.2. Electron paramagnetic resonance

To better understand the oxidation states of transition metal elements in pristine material P2-$Na_{0.67}Ni_{0.33}Mn_{0.67}O_2$ and the aliovalently V-substituted materials, electron paramagnetic resonance studies have been carried out (Fig.2). For stoichiometric composition $Na_{0.67}Ni_{0.33}Mn_{0.67}O_2$, the oxidation states of Ni and Mn can be elucidated as +2 and +4, maintaining charge neutrality. Both $Ni^{2+}$and Mn^{4+}-ions are paramagnetic with spins states of S=1 and S=3/2. However, the conventional EPR spectroscopy (X-band) cannot resonate the ions with integer-spin ground states due to the higher magnitude of the zero-field splitting parameter. Therefore, Ni^{2+} remains as EPR silent at a 9.6 GHz absorption signal [34]. V^{5+} dopants in the materials $Na_{0.67}Ni_{0.33-x}V_xMn_{0.67}O_2$ (x= 0.05 and 0.11) can be eliminated from paramagnetic consideration due to the presence of zero d-electron. This phenomenon reflects in the EPR spectra as all of these compounds, displaying a single Lorentzian line due to only Mn^{4+}-ion. For $Na_{0.67}Ni_{0.33}Mn_{0.67}O_2$, containing only Mn^{4+}-ions, the electron paramagnetic resonance spectrum consists of a Lorentzian line with a g-value of 1.9917 and a line-width ΔH_{pp} of 137.9 mT, as shown in Fig.2. $Na_{0.67}Ni_{0.22}V_{0.11}Mn_{0.67}O_2$ contains a mix of Mn^{4+} and Mn^{3+}-ion, resulting in a significant line broadening of the EPR spectra, reaching a value of 184.7 mT. Also, as expected for the mixed-phase scenario, the g-factor deviates strongly from 1.9917 to approaching a value of 1.9765. EPR line width and g-factor of $Na_{0.67}Ni_{0.28}V_{0.05}Mn_{0.67}O_2$ are recorded as 171.9 mT and 1.9783, respectively. The EPR spectral characteristics and the calculated average oxidation states of Mn are listed in Table 1.

The V-substitution on the Ni- site ($Na_{0.67}Ni_{0.33-x}V_xMn_{0.67}O_2$) was done to follow the effect of Mn^{3+}-ions on the electrochemical performances of the materials. The Mn^{3+}/Mn^{4+}ions were further confirmed using EPR studies. The V-substitution (x= 0.05, 0.11) varied the Mn^{4+}/ Mn^{3+}-ion ratio from 1:0 ($Na_{0.67}Ni_{0.33}Mn_{0.67}O_2$) to 3:1 ($Na_{0.67}Ni_{0.28}V_{0.05}Mn_{0.67}O_2$) and to 1:1 ($Na_{0.67}Ni_{0.22}V_{0.11}Mn_{0.67}O_2$). EPR spectral results confirm the oxidation states of Mn on V-substitution. The increase in Mn^{3+}-ion in the compound results in spectral line broadening and

reduced g-value in V-substituted materials compared to the parent NNMO. P2-$Na_{0.67}Ni_{0.22}V_{0.11}Mn_{0.67}O_2$ having the maximum Mn^{3+} / Mn^{4+} ion ratio, displays the most broadened EPR spectral line and the least g-value, whereas the parent P2-type $Na_{0.67}Ni_{0.33}Mn_{0.67}O_2$ shows the minimum spectral broadening and the highest g-value. EPR line-width and g-factor for $Na_{0.67}Ni_{0.28}V_{0.05}Mn_{0.67}O_2$ lie in between, as listed in Table 1.

Table 1: List of EPR line-width (ΔH_{pp}) and g-factor for $Na_{0.67}Ni_{0.33-x}V_xMn_{0.67}O_2$ with varying x-value.

x-value	**Oxidation state of Mn (Calculated)**	**(ΔH_{pp}) value (G)**	**g-value, g=(hν)/(μB)**
0	~ 3.98	1378.93297	1.9917
0.05	~ 3.75	1719.52259	1.9783
0.11	~ 3.49	1846.78523	1.9765

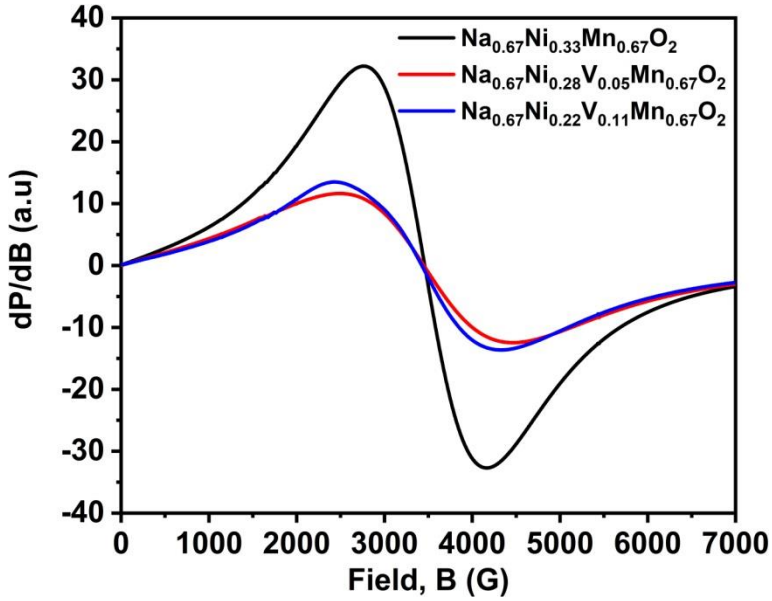

Fig.2: Electron paramagnetic resonance spectra of P2-$Na_{0.67}Ni_{0.33-x}V_xMn_{0.67}O_2$ samples where x= 0, 0.05 and 0.11.

3.1.3. Raman spectroscopy

P2-type $Na_{0.67}Ni_{0.33-x}V_xMn_{0.67}O_2$ belongs to space group $P6_3/mmc$, the Raman and IR spectroscopy results can be correlated to hexagonal P2-type Na_xCoO_2 [35]. From molecular symmetry point, Na_xCoO_2 falls into D_{6h} point group. Raman active phonon modes of such group are predicted as A_{1g}, E_{2g}, and E_{1g} considering active spectroscopy components of the group character table. The vibration of only oxygen atoms follows the A_{1g} and E_{1g} modes, whereas three E_{2g} modes reflect the vibrations of both sodium and oxygen atoms. Four typical Raman peaks can be identified for all materials synthesized in molecular formula $Na_{0.67}Ni_{0.33-x}V_xMn_{0.67}O_2$ (where x = 0, 0.05, and 0.11) with varying x-values, as shown in Fig.3. The most intense peak at 485 cm^{-1} corresponds to one of the three E_{2g} modes in the pristine material. The peak at 593 cm^{-1} reflects A_{1g} mode associating

with the stretching vibrations from the oxygen present in the adjacent layers parallel to the c-axis. On the other hand, the E_{2g} and E_{1g} modes correspond to atomic displacement perpendicular to the c-axis. Although there is no evident change in the XRD patterns of aliovalently doped samples, the Raman spectra show some differences in the V-substituted and pristine samples. There is peak broadening of Raman spectral lines for all the V-substituted samples for two reasons - the inclusion of more Jahn-Teller active Mn^{3+}-ions by V-substitution induces sub-lattice formation in the matrix. Furthermore, peak broadening in polycrystalline samples can occur due to a higher degree of lattice disorder in the V-substituted $Na_{0.67}Ni_{0.33}Mn_{0.67}O_2$.

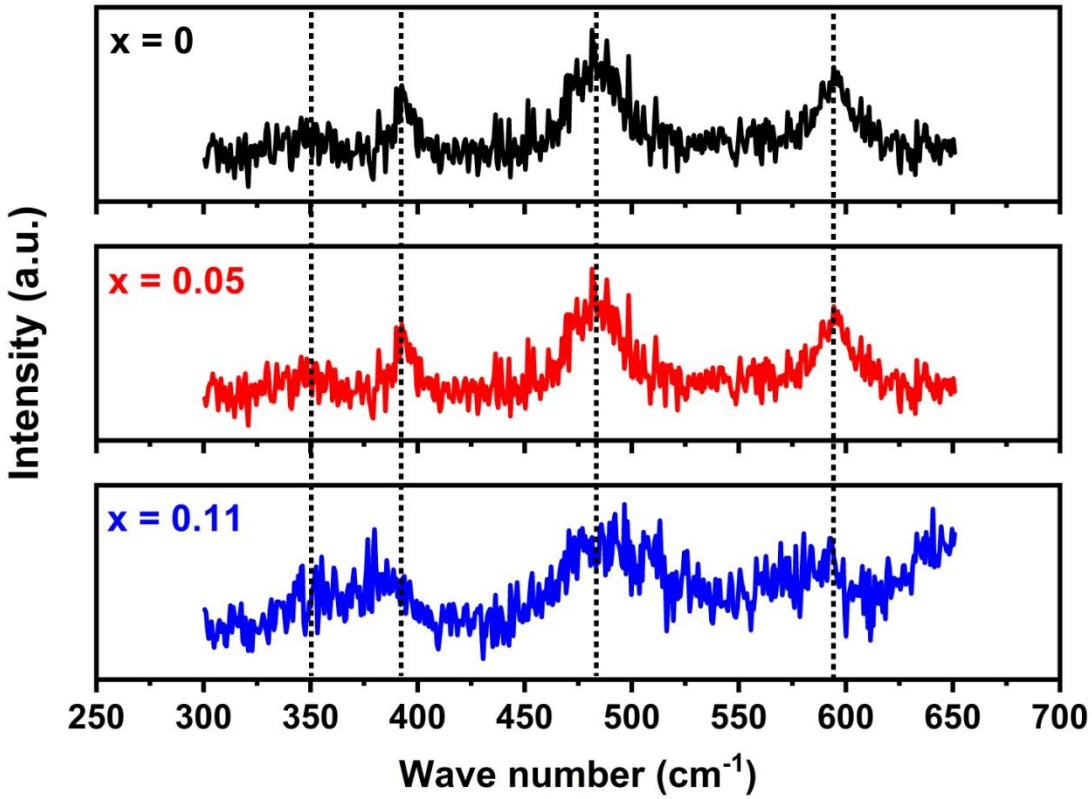

Fig.3: Raman spectra of P2-$Na_{0.67}Ni_{0.33-x}V_xMn_{0.67}O_2$ samples (where x= 0, 0.05 and 0.11). The dotted lines show the peak positions.

3.1.4. Scanning electron microscopy (SEM) images and Energy-dispersive X-ray spectroscopy (EDX)

Fig. SI 1 shows the change in surface morphologies upon V-doping in the Ni-site of P2-type $Na_{0.67}Ni_{0.33}Mn_{0.67}O_2$. All of the micrographs reveal that irregular shapes of micrometer-sized particles from the electrode surfaces. Moreover, traces of all the elements present in the structural formula have been found in EDX analysis in a nearly similar atomic percentage ratio (Fig. SI 2).

3.2. Electrochemical characterization

3.2.1. Cyclic voltammetry

The electrochemical performance of P2-type $Na_{0.67}Ni_{0.33}Mn_{0.67}O_2$ can be controlled by choosing the different voltage ranges for the charge-discharge cycles, especially the upper cut-off voltage [36]. Incidentally, both the high voltage (>4.2 V) and low voltage (<2 V) cut-offs can influence

the structural transitions in the cathode, significantly affecting the capacity retention and cyclic stability of the cathode [37, 38]. When P2-type layered oxides are charged above 4.1 V, an irreversible phase transition (from P2 to O2-phase) leads to a high capacity loss in the initial cycles. Upon deep charging (> 4.1V), the lesser Na^+ ions between the TMO_6 oxide layers lead to lesser screening of O2--O2- repulsions. TMO_6 oxide sheets are forced to glide and control the repulsion resulting from the shrinkage in the inter-slab distance. In addition, Na-ion vacancies are more stable in the octahedral sites than that of prismatic sites. As a result, a transition of P2-O2-phase is apparent at the end of the charge. The O2-phase follows an ABAC stacking pattern of oxygen, and the Na-ion vacancies occupy the octahedral sites. Although most P2-type materials P2-O2 transition upon charging, a few other structural transitions are also reported. Mn-Fe based binary Na_xTMO_2 shows the formation of an intermediate OP4-phase upon charging instead of O2-phase to overcome the thermodynamic instability from the oxide layer glide [39]. OP4-phase shows stacking faults along the c-axis direction and is observed during the high voltage charging of P2-type Na_xTMO_2 compounds [40-42]. Aliovalent substitution at the transition metal site assists the formation of thermodynamically stable OP4-phase and helps the reversibility of the charge-discharge reaction [43, 44].

Therefore, to understand the effect of aliovalent doping on the electrochemical properties, by altering the Mn^{3+}/Mn^{4+}-ion ratio, the voltage range of operation is limited within 1.5 - 4.1 V. Cyclic voltammetry of P2-type$Na_{0.67}Ni_{0.33}Mn_{0.67}O_2$ (Fig. 4a) reveals two consistent peaks at 3.5 V and 3.8 V in the oxidation range starting from the first cycle. These two peaks arise from the Ni^{2+}/Ni^{3+} and Ni^{3+}/Ni^{4+} oxidation on Na^+-ion de-intercalation. Interestingly, a small peak at 2.5 V from the Mn^{3+}/Mn^{4+} redox appears and starts fading with more Na^+-ion intercalation. A new peak that starts to appear at 2.2 V during cycling is from the improved repeatability of the Mn^{3+}/Mn^{4+} redox. Cyclic voltammetry of $Na_{0.67}Ni_{0.33-x}V_xMn_{0.67}O_2$ (x = 0.05 and 0.11) reveals a distinct redox mechanism dominated by Mn^{3+}/Mn^{4+} redox, and the Ni^{2+}/Ni^{4+} redox peaks almost disappear, leading to a solid-solution type behavior (Fig. 4b and 4c).

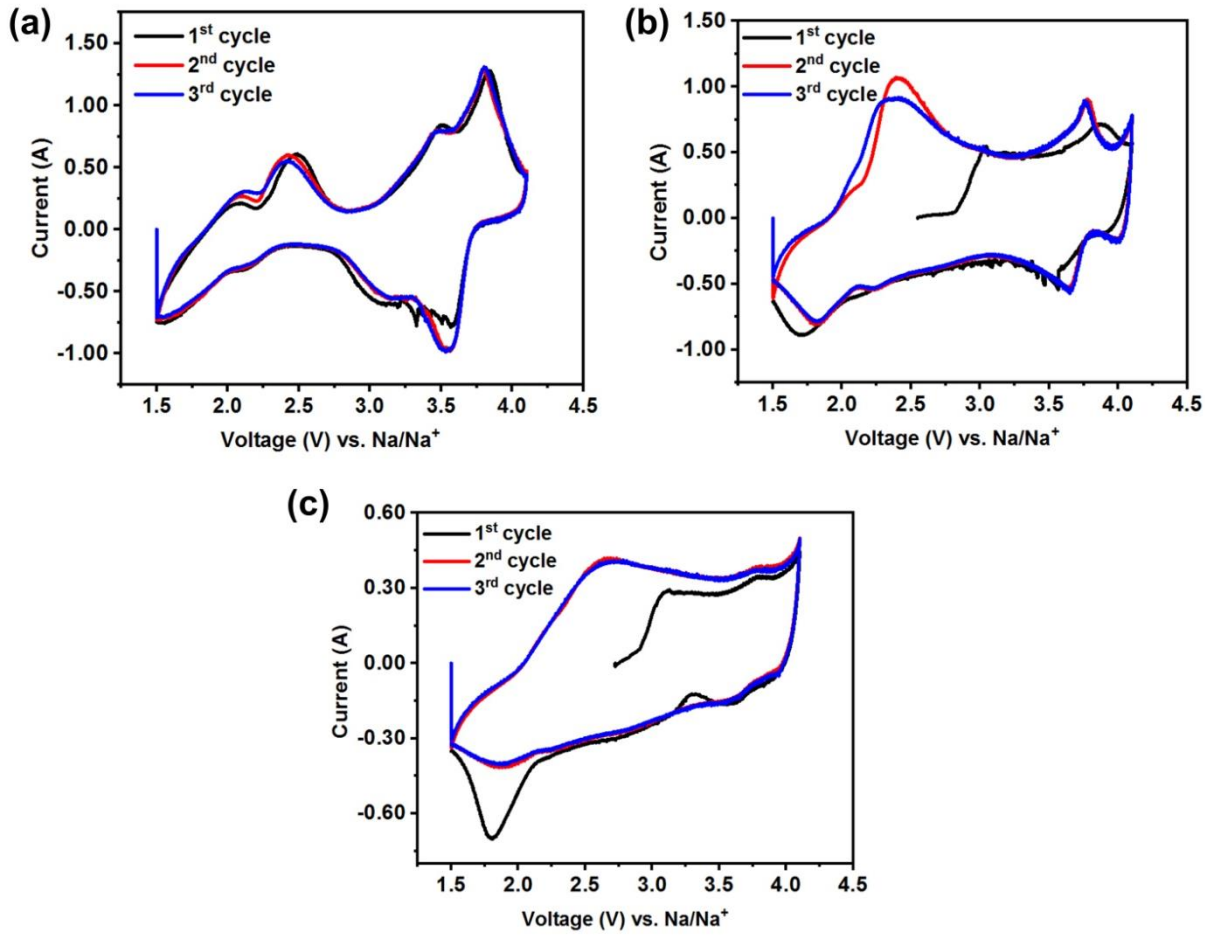

Fig. 4: Cyclic voltammograms at a scan rate of 1 mVs^{-1} of $Na_{0.67}Ni_{0.33-x}V_xMn_{0.67}O_2$ electrode half-cells where (a) x=0, (b) x=0.05 and (c) x=0.11 between 1.5 and 4.1 V.

Fig. 5a-c reflects the cyclic voltammograms of $Na_{0.67}Ni_{0.33-x}V_xMn_{0.67}O_2$ (x = 0, 0.05 and 0.11) electrodes when cycled between 1.5 and 4.3 V. As mentioned earlier, the pristine P2-type $Na_{0.67}Ni_{0.33}Mn_{0.67}O_2$ exerts an irreversible redox peak above 4.2 V. A pair of redox peaks located near 4.25/3.9 V confirms the presence of P2- to O2-phase transformation. The Ni^{2+}/Ni^{3+}, $Ni^{3+}/Ni^{4+,}$ and Mn^{3+}/Mn^{4+} redox peaks appear at 3.4/3.25, 3.75/3.5, and 2.75/2.0 V, respectively. The V-substituted $Na_{0.67}Ni_{0.28}V_{0.05}Mn_{0.67}O_2$ electrode shows three distinct redox peaks at 2.5/2.0, 3.75/3.6, and 4.2/4.0 V for Mn^{3+}/Mn^{4+}, $Ni^{2+}/Ni^{4+,}$ and the P2-O2 structural transition, respectively. The high voltage redox peak (4.2/4.0 V) has improved compared to the parent $Na_{0.67}Ni_{0.33}Mn_{0.67}O_2$ electrode. The first two cycles almost overlap in the higher voltage region, but slight irreversibility is observed from the third cycle. On the contrary, the higher V-substituted sample, $Na_{0.67}Ni_{0.22}V_{0.11}Mn_{0.67}O_2$ electrode, shows the best reversibility of the high voltage redox peaks. Apart from the high voltage peak, the cyclic voltammograms of the $Na_{0.67}Ni_{0.22}V_{0.11}Mn_{0.67}O_2$ electrode do not exhibit any sharp redox transition peaks. The broad peaks observed in the CV revealed a solid-solution behavior which explains the improved electrochemical cycle stability of the higher V-substituted $Na_{0.67}Ni_{0.22}V_{0.11}Mn_{0.67}O_2$ electrodes.

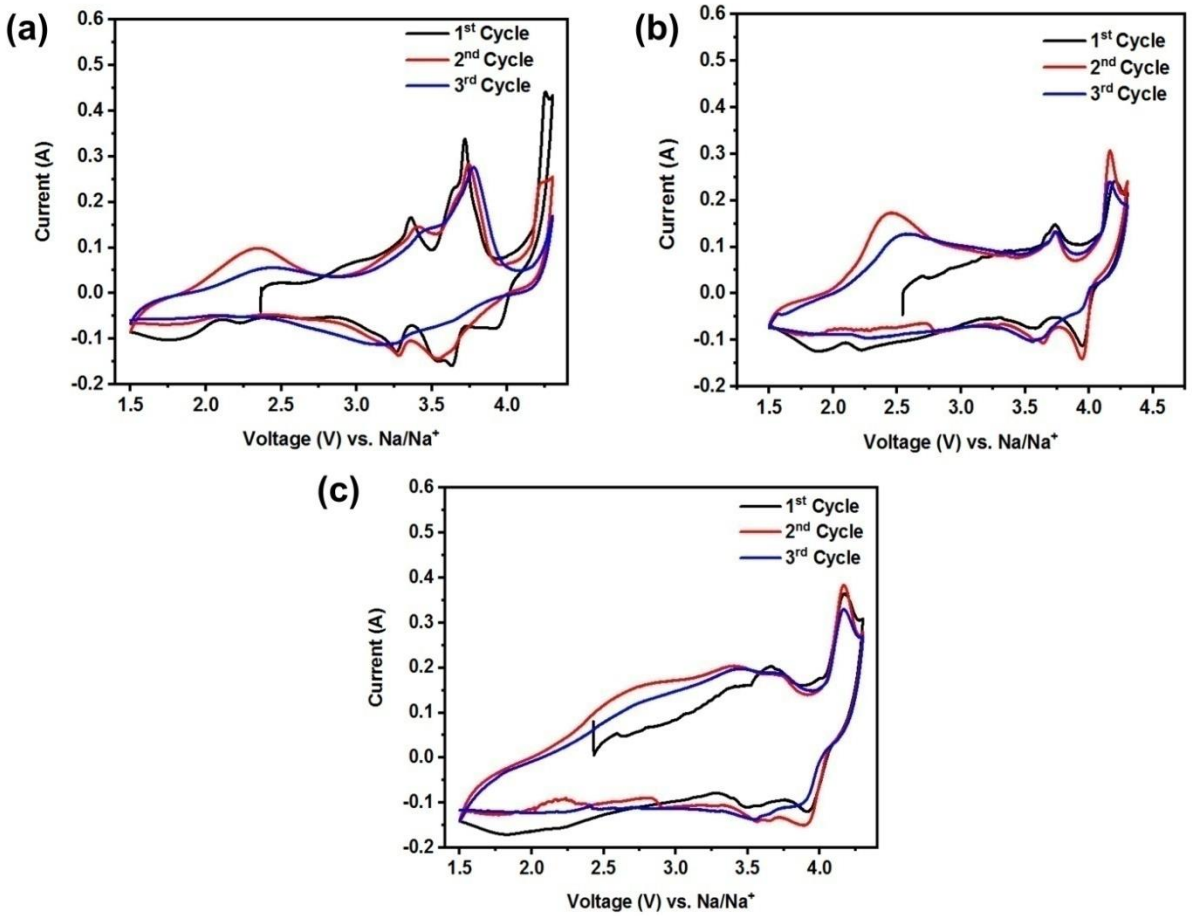

Fig. 5: Cyclic voltammograms at a scan rate of 0.1 mVs^{-1} of $Na_{0.67}Ni_{0.33-x}V_xMn_{0.67}O_2$ electrode half-cells where (a) x= 0, (b) x= 0.05 and (c) x= 0.11 between 1.5 and 4.3 V.

3.2.2. Galvanostatic charge-discharge measurements

P2-type $Na_{0.67}Ni_{0.33}Mn_{0.67}O_2$ exhibits an initial discharge capacity of 123 $mAhg^{-1}$ at a voltage range of 1.5-4.1 V (Fig. 6a) at a rate of 0.05C. The charge-discharge profile shows multiple structural transitions due to different Na^+-ion/vacancy ordering at various Na-stoichiometries. Charge-discharge profiles of$Na_{0.67}Ni_{0.28}V_{0.05}Mn_{0.67}O_2$ (Fig. 6b) display an initial discharge capacity of 138 $mAhg^{-1}$ at a rate as slow as 0.05C. The discharge curve shows two-phase transformations corresponding to two voltage plateaux at ~3.7 V and ~2 V in agreement with the Ni^{2+}/Ni^{4+} and Mn^{3+}/Mn^{4+} redox reactions observed in the CV (Fig. 4a). The more significant contribution from Mn^{3+}/Mn^{4+} redox, the charge-discharge characteristics of $Na_{0.67}Ni_{0.22}V_{0.11}Mn_{0.67}O_2$ material in the voltage range of 1.5-4.1 V (Fig. 6c) indicates a unique solid-solution type behavior with further enhanced initial discharge capacity of 146 $mAhg^{-1}$ at a rate of 0.05C. The capacity fades to 50% of its initial capacity in the first 30 cycles showing poor reversibility of Na-ion intercalation/de-intercalation. Also, the average potential of P2-type $Na_{0.67}Ni_{0.33-x}V_xMn_{0.67}O_2$ electrodes (x = 0.05 and 0.11) falls from 3.2 V (in P2- $Na_{0.67}Ni_{0.33}Mn_{0.67}O_2$) to 2.5 and 2.75 V respectively. Such a drop in average working potential occurs owing to the impedance buildup at the electrode surface. Hence, V-doped electrodes fail to overcome the resistance arising at the interface. An incremental capacity plot for the first five charge-discharge cycles indicates the superiority of the pristine electrode between 1.5 and 4.1 V operating range (inset of Fig. SI 3a). The poorer capacity retention of V-substituted P2-type $Na_{0.67}Ni_{0.33-x}V_xMn_{0.67}O_2$ electrodes is due to the influence of more Jahn-Teller distortion Mn^{3+}-ion present in the substituted compounds.

Aliovalent substitution is reported to partially or fully suppress the P2-O2 phase transition, which appears at upper cut-off voltages >4.2 V in P2-type $Na_{0.67}Ni_{0.33}Mn_{0.67}O_2$ [43, 44]. V-substituted P2-type $Na_{0.67}Ni_{0.33-x}V_xMn_{0.67}O_2$ electrodes (x= 0.05 and 0.11) are further cycled between 1.5 and 4.3 V in order to mask the P2-O2 structural transition for better cyclic stability/capacity retention (Fig. 7a-c). P2-O2 structural transition is evident in P2-type $Na_{0.67}Ni_{0.33}Mn_{0.67}O_2$ electrodes in the form of a long voltage plateau at 4.2 V. The P2-O2 irreversible transitions that exist for the initial cycles significantly affect the capacity retention in these types of materials [20, 43]. As seen from Fig. 7, the high voltage plateau fades with successive cycles causing poor capacity retention in the charge-discharge profiles. The parent $Na_{0.67}Ni_{0.33}Mn_{0.67}O_2$ barely retains 50% of its initial discharge capacity after the first ten cycles. Interestingly, such voltage plateau shortens in the $Na_{0.67}Ni_{0.28}V_{0.05}Mn_{0.67}O_2$ electrode, indicating a partially suppressed P2-O2 transition (as shown in Fig. SI 4). The capacity contribution of the P2-O2 phase transition is ~ 31 $mAhg^{-1}$ in the $Na_{0.67}Ni_{0.28}V_{0.05}Mn_{0.67}O_2$ electrode compared to ~ 80 $mAhg^{-1}$ for the parent P2-$Na_{0.67}Ni_{0.33}Mn_{0.67}O_2$electrode. The initial discharge capacity ~122.3$mAhg^{-1}$, which is 25 $mAhg^{-1}$ lower than the parent $Na_{0.67}Ni_{0.33}Mn_{0.67}O_2$ material. The lesser amount of electrochemically active Ni^{2+}-ion (substituted V-ion is electrochemically inactive) reduces the initial discharge capacity. The lower substituted sample shows poor capacity retention as compared to the parent P2-type $Na_{0.67}Ni_{0.33}Mn_{0.67}O_2$. On the other hand, $Na_{0.67}Ni_{0.22}V_{0.11}Mn_{0.67}O_2$ electrodes are found to be superior in capacity retention. $Na_{0.67}Ni_{0.22}V_{0.11}Mn_{0.67}O_2$ electrodes also deliver a high initial

discharge capacity of 155.2 $mAhg^{-1}$ when cycled between 1.5 and 4.3 V. The higher initial discharge capacity comes from the P2-O2 high voltage phase transition as well as the Mn^{3+}/Mn^{4+}-redox at lower voltages. Although the P2-O2 structural transition happens at least in the first charge cycle of the $Na_{0.67}Ni_{0.22}V_{0.11}Mn_{0.67}O_2$ electrodes, the retention is better with ~76.1% of the discharge capacity retained after the initial ten cycles. The range of P2-O2 phase transition and its contribution towards the specific capacity of $Na_{0.67}Ni_{0.22}V_{0.11}Mn_{0.67}O_2$electrodes ($1^{st}$ charge cycle) is shown in Fig. SI 4. A complete solid-solution type behavior of $Na_{0.67}Ni_{0.22}V_{0.11}Mn_{0.67}O_2$ electrode with a higher ion-transport dynamics [45, 46] is responsible for the improved capacity retention in the charge-discharge cycles. The charge-discharge profiles of $Na_{0.67}Ni_{0.33-x}V_xMn_{0.67}O_2$ (x = 0, 0.05 and 0.11) half-cells at a rate of 0.1C between 1.5 and 4.3 V are shown in Fig. 7.

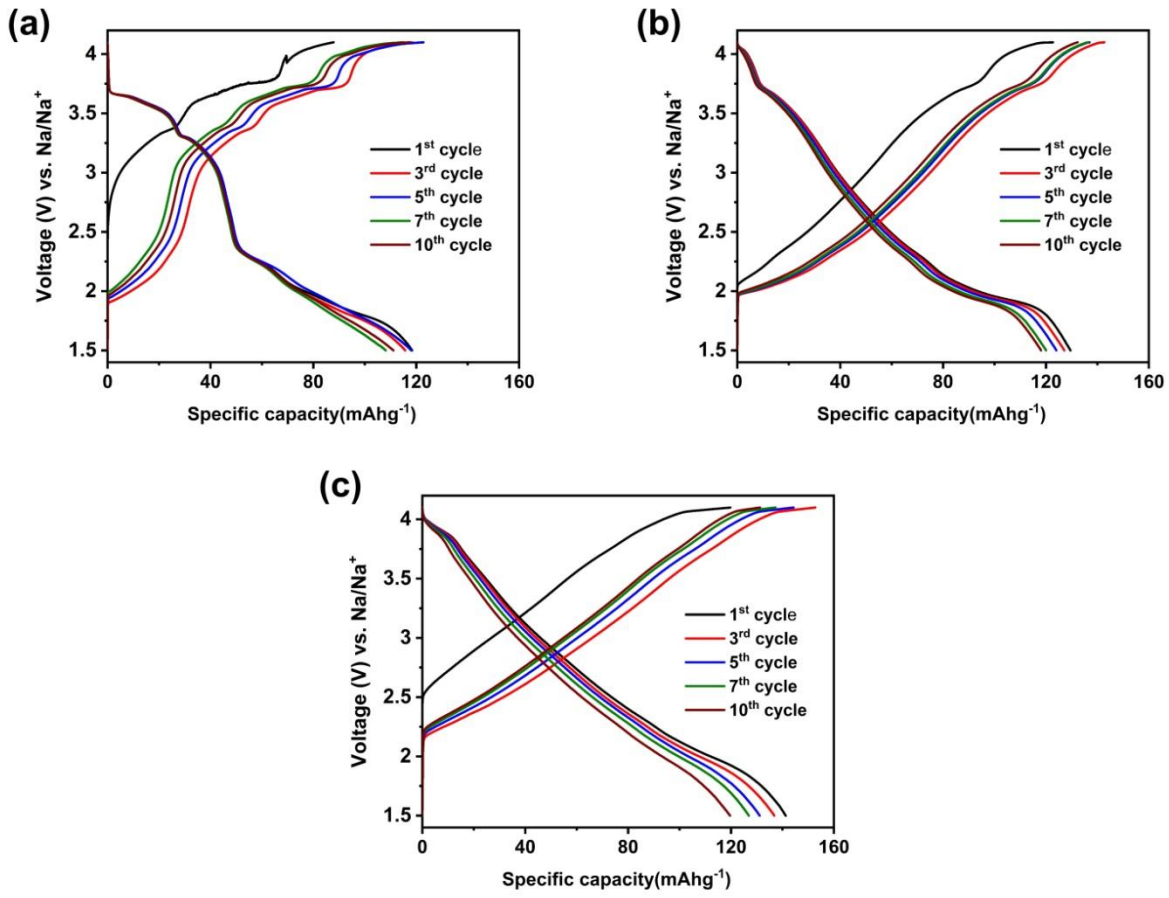

Fig.6: Charge-discharge profiles of $Na_{0.67}Ni_{0.33-x}V_xMn_{0.67}O_2$ electrode half-cells where (a) x= 0, (b) x= 0.05 and (c) x= 0.11 at a rate of 0.05C between 1.5 and 4.1 V.

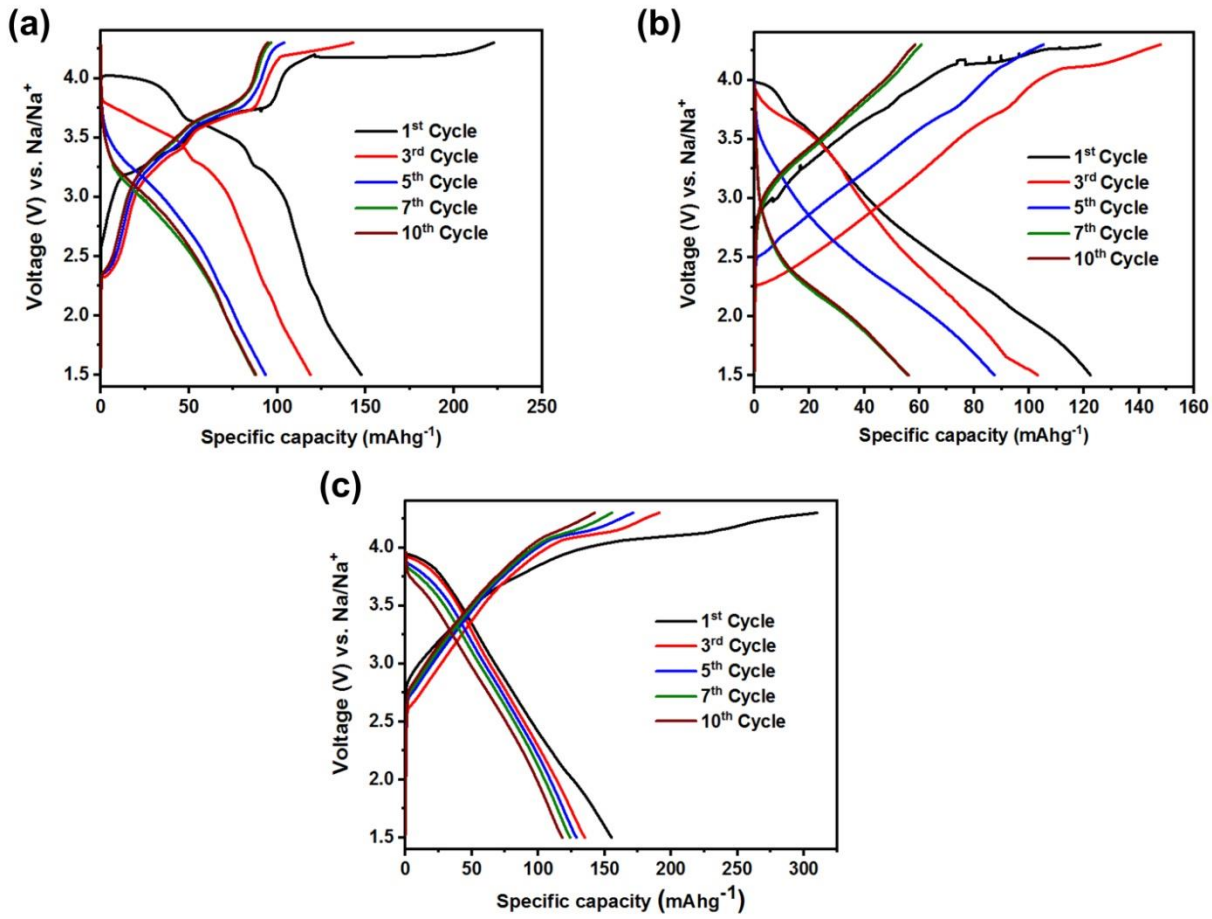

Fig.7: Charge-discharge profiles of $Na_{0.67}Ni_{0.33-x}V_xMn_{0.67}O_2$ electrode half-cells where (a) x= 0, (b) x= 0.05 and (c) x= 0.11 at a rate of 0.1C between 1.5 and 4.3 V.

The cycle stability characteristics of P2-type $Na_{0.67}Ni_{0.33-x}V_xMn_{0.67}O_2$ electrodes at different cut-off voltage ranges are shown in Fig. 8. However, V-substituted materials' reversibility is inferior to that of the pristine material between 1.5-4.1 V. The parent $Na_{0.67}Ni_{0.33}Mn_{0.67}O_2$ shows a 10% capacity loss only (Fig. 8a) for the initial 50 cycles. On the contrary, $Na_{0.67}Ni_{0.28}V_{0.05}Mn_{0.67}O_2$ and $Na_{0.67}Ni_{0.22}V_{0.11}Mn_{0.67}O_2$ electrodes retained 34% and 42% of the initial discharge capacities at the end of the 50^{th} cycle. Such loss of reversible capacities in V-substituted $Na_{0.67}Ni_{0.33-x}V_xMn_{0.67}O_2$ (where x = 0.05 and 0.11) electrode half-cells arises from the presence of Jahn-Teller active Mn^{3+}-ions. From the stoichiometry, the ratio of Mn^{3+}/Mn^{4+}ions increases from 0:1 in the parent material to 1:3 at x = 0.05, and 1:1 at x is 0.11. A greater extent of Jahn-Teller active Mn^{3+}-ions disturbs the structural reversibility of the $Na_{0.67}Ni_{0.28}V_{0.05}Mn_{0.67}O_2$ electrodes when compared to the pristine $Na_{0.67}Ni_{0.33}Mn_{0.67}O_2$. Surprisingly, slightly better capacity retention in $Na_{0.67}Ni_{0.22}V_{0.11}Mn_{0.67}O_2$ electrodes is observed due to the purely solid-solution type behavior observed in the charge-discharge curves.

Further, to understand the effect of V-substitution of P2-O2 transition at high voltages

and the capacity retention, $Na_{0.67}Ni_{0.33-x}V_xMn_{0.67}O_2$ electrodes were studied between 1.5 and 4.3 V. An extended upper cut-off voltage till 4.3 V resulted in a slight improvement in capacity retention in a 50 charge-discharge cycle range as compared to the narrow voltage range (1.5 - 4.1 V). The $Na_{0.67}Ni_{0.22}V_{0.11}Mn_{0.67}O_2$ electrodes showed retention of 62% of the initial discharge capacity after the 50^{th} charge-discharge cycle at a rate of 0.1C, whereas the parent material retained 64% of its initial capacity. The $Na_{0.67}Ni_{0.28}V_{0.05}Mn_{0.67}O_2$ electrode retained 67% of its initial discharge capacity after 50 charge-discharge cycles. Although a sharp capacity fading is evident in the initial cycles, the $Na_{0.67}Ni_{0.28}V_{0.05}Mn_{0.67}O_2$ electrode manages to exhibit the maximum capacity retention in this range.

Upon extending the voltage limit to 4.3 V, $Na_{0.67}Ni_{0.33}Mn_{0.67}O_2$ experiences an irreversible P2-O2 phase transition which deteriorates its cycle stability. However, the sample $Na_{0.67}Ni_{0.22}V_{0.11}Mn_{0.67}O_2$ can successfully suppress this transition and offer a slow capacity fading in the charge-discharge cycles evident by comparing Fig. 7a-c 8a and 8b and inset of Fig. SI 3b.

The C-rate capabilities of $Na_{0.67}Ni_{0.33-x}V_xMn_{0.67}O_2$ samples (where x= 0, 0.05 and 0.11) are shown in Fig. 8c at C-rates 0.05C, 0.1C, 0.2C and 0.5C between 1.5–4.1 V. Both V-substituted electrodes display poor rate kinetics at faster current cycling. Lower V-substituted $Na_{0.67}Ni_{0.28}V_{0.05}Mn_{0.67}O_2$ electrodes offer specific discharge capacity as low as 21 $mAhg^{-1}$ at a rate of 0.5C. $Na_{0.67}Ni_{0.22}V_{0.11}Mn_{0.67}O_2$ half-cells deliver ~ 36 $mAhg^{-1}$ at the same C-rate. The V-substituted $Na_{0.67}Ni_{0.33-x}V_xMn_{0.67}O_2$ electrodes show poor rate performances as compared to the pristine material. Similar behavior was observed when Ni-site was substituted by Ti^{4+}-ions [20]. Ti-substituted $Na_{0.67}Ni_{0.33-x}Ti_xMn_{0.67}O_2$ electrodes (x = 0.08 and 0.16) have displayed better C-rate performances only at capacity rates higher than 0.5C. The higher Ti-substituted electrode shows better rate capabilities than the lower substituted sample at all C-rates between 1.5 and 4.3 V. V-substituted electrodes also follow a similar trend. However, the rate capabilities in Ti-substituted electrodes are found to be slightly superior as compared to the V-substituted sample. Ti-substituted $Na_{0.67}Ni_{0.33-x}Ti_xMn_{0.67}O_2$ electrodes (x = 0.08 and 0.16) have furnished specific capacities above 60 $mAhg^{-1}$ at a rate of 0.5C whereas the specific discharge capacities of $Na_{0.67}Ni_{0.33-x}V_xMn_{0.67}O_2$ electrodes (x = 0.05 and 0.11) are limited below 20 $mAhg^{-1}$ at the same C-rate. The decreased inter-layer spacing (d_{002}) with increasing Ti and V-substitution restricts faster Na^+-ion diffusion at higher C-rates. Interestingly, the V^{5+}-ions (ionic radii 0.54 Å) are 0.07 Å smaller than Ti^{4+}-ions (ionic radii 0.61 Å). Therefore, a larger reduction of lattice size is obvious upon V-substitution in $Na_{0.67}Ni_{0.33}Mn_{0.67}O_2$. Such lattice shrinkage upon V-substitution in $Na_{0.67}Ni_{0.33}Mn_{0.67}O_2$ was confirmed in the X-ray diffraction patterns (Fig. 1). The material regains its capacity at a lower 0.05C rate, clearly hinting at the kinetic limitations in the material (Fig. 8c and 8d). $Na_{0.67}Ni_{0.28}V_{0.05}Mn_{0.67}O_2$ electrodes reach a specific capacity of 137 $mAhg^{-1}$ when the rate is decreased from 0.5C to 0.05C, as shown in Fig. 8c. On the contrary, the parent $Na_{0.67}Ni_{0.33}Mn_{0.67}O_2$ electrode starts to perform poorly at a slower C-rate due to the P2-O2 phase transition when cycled between 1.5 and 4.3 V (Fig. 8d).

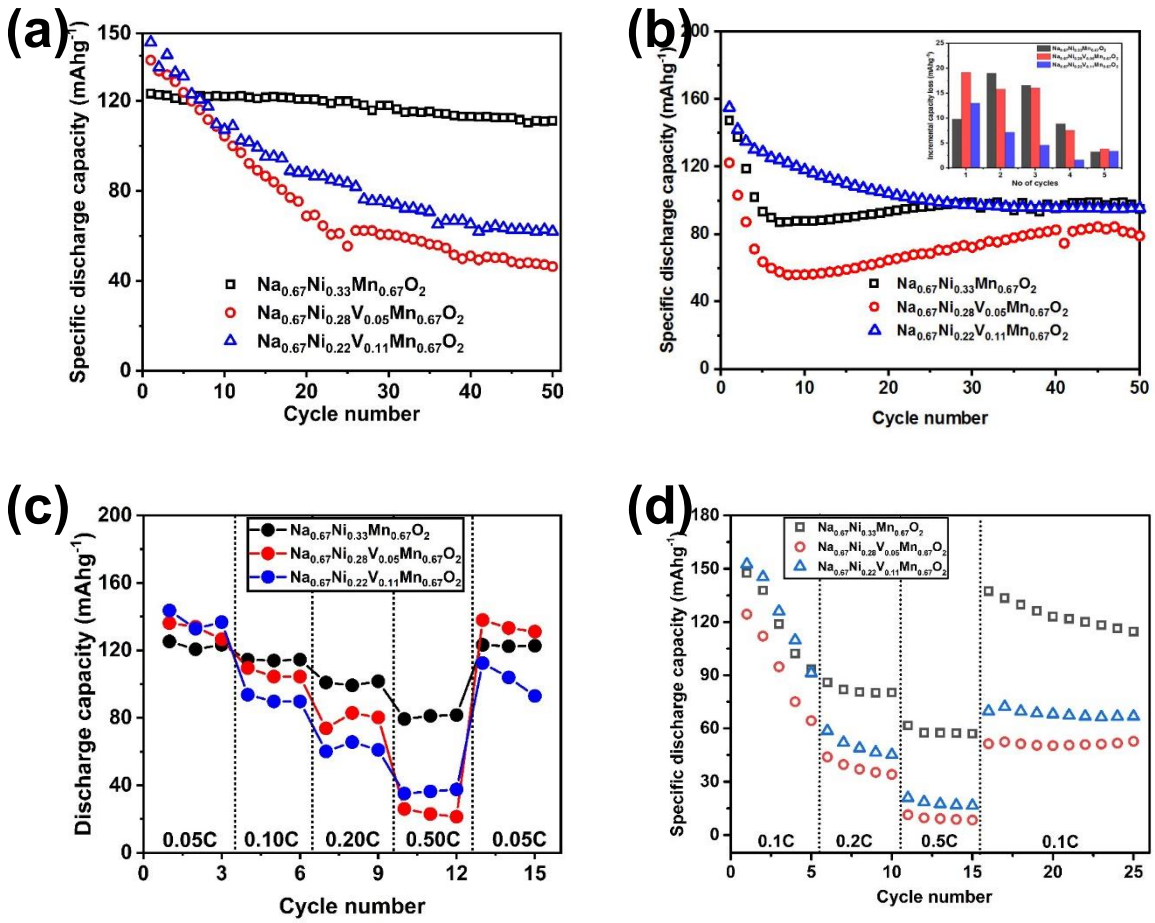

Fig.8: Cycle stabilities of P2-type $Na_{0.67}Ni_{0.33-x}V_xMn_{0.67}O_2$ samples (where x= 0, 0.05 and 0.11) (a) at the rate of 0.05 C between 1.5- 4.1 V and (b) at the rate of 0.1 C between 1.5- 4.3 V. Rate performances of P2-type$Na_{0.67}Ni_{0.33-x}V_xMn_{0.67}O_2$ samples (where x= 0, 0.05 and 0.11) (c) at the rate of 0.05C, 0.1C, 0.2C and 0.5C between 1.5 and 4.1 V and (d) at the rate of 0.1C, 0.2C and 0.5C between 1.5 and 4.3 V.

The cycle stabilities of P2-type $Na_{0.67}Ni_{0.33-x}V_xMn_{0.67}O_2$ electrodes (x = 0, 0.05 and 0.11) were optimized further in different organic ester-based electrolyte systems. Four different electrolyte systems with compositions - Ethylene carbonate (EC): Propylene carbonate (PC): Dimethyl carbonate (DMC) (0.45: 0.45: 0.1), Ethylene carbonate (EC): Diethyl carbonate (DEC) (1: 1), Ethylene carbonate (EC): Propylene carbonate (PC) (1: 1) and Propylene carbonate (PC) were used. The sodium salt remained the same (1.0 M $NaClO_4$). EC: DEC (1: 1) mixture is popularly known for its electrochemical voltage stability compared to the conventional only PC electrolyte [47]. At the same time, the EC: PC (1: 1) combination is one reason for better capacity retention due to EC-induced stable SEI formation on the anode surface [48]. Additionally, as mentioned earlier, the addition of 10% DMC into the EC: PC mixture gives rise to enhanced ionic conductivity and lesser viscosity [33]. Hence, a comparative study among the above three electrolyte combinations with PC on NNMO was carried out.

The electrodes were cycled at the rate of 0.2 C between 1.5 and 4.3 V. Pristine P2-type

$Na_{0.67}Ni_{0.33}Mn_{0.67}O_2$ exhibits the highest initial specific capacity in all the electrolyte combinations. The initial specific capacity decreases upon V-substitution. The lattice shrinkage caused by the inclusion of smaller-sized V^{5+}-ions results in lower capacity at a rate of 0.2C. Also, on moving from $Na_{0.67}Ni_{0.33}Mn_{0.67}O_2$ to $Na_{0.67}Ni_{0.22}V_{0.11}Mn_{0.67}O_2$, a significant increase in the extent Mn^{3+}-ions is expected. Herein, a continuous increase of Jahn-Teller active Mn^{3+}-ions upon V-substitution leads to structural instability, further adding to the deterioration of capacity retention. As a whole, both V-substituted $Na_{0.67}Ni_{0.33-x}V_xMn_{0.67}O_2$ electrodes (x = 0.05 and 0.11) present poor capacity retention as compared to the parent P2-type $Na_{0.67}Ni_{0.33}Mn_{0.67}O_2$. All three P2-type $Na_{0.67}Ni_{0.33-x}V_xMn_{0.67}O_2$ electrodes show the poorest capacity retention in the presence of 1.0 M $NaClO_4$ in PC electrolyte (Fig. 9d). The initial discharge capacities and capacity retention percentages were recorded as 136.9, 106.6, and 101.8 $mAhg^{-1}$ and 19%, 13%, and 32% over 50 charge-discharge cycles for x= 0, 0.05 and 0.11 electrodes respectively. The best capacity retention for V-substituted electrode $Na_{0.67}Ni_{0.22}V_{0.11}Mn_{0.67}O_2$ has been observed in the case of 1.0 M $NaClO_4$ in Ethylene carbonate: Propylene carbonate: Dimethyl carbonate (0.45: 0.45: 0.1) electrolyte as shown in Fig. 9a. $Na_{0.67}Ni_{0.33-x}V_xMn_{0.67}O_2$ electrodes (x= 0, 0.05 and 0.11) has achieved initial discharge capacities up to 120.4, 112.5 and 104.9 $mAhg^{-1}$ respectively. The cycle stabilities were calculated as 71%, 38%, and 79% over 50 charge-discharge cycles, respectively.
Interestingly, the evolution of specific capacities with charge-discharge cycles in the parent P2-type $Na_{0.67}Ni_{0.33}Mn_{0.67}O_2$ electrode follows a unique trend in the case of 1.0 M $NaClO_4$ in EC:DEC and EC:PC solvents. The specific capacity initially drops to 5 cycles, increases to about 30 cycles, and eventually decreases slowly. The initial drop of capacity observed due to the increased degree of polarization and the consequent increase in the capacity due to activation of the electrode surface is reported earlier [49, 50]. A stable SEI formation by EC-based electrolytes causes an increase in the active electrochemical sites upon repeated cycling, enhancing the specific capacity. However, after about 30 cycles, the increased polarization eventually fades the specific capacity leading to an overall capacity loss of about 25% (EC: PC) and 14% (EC: DEC).

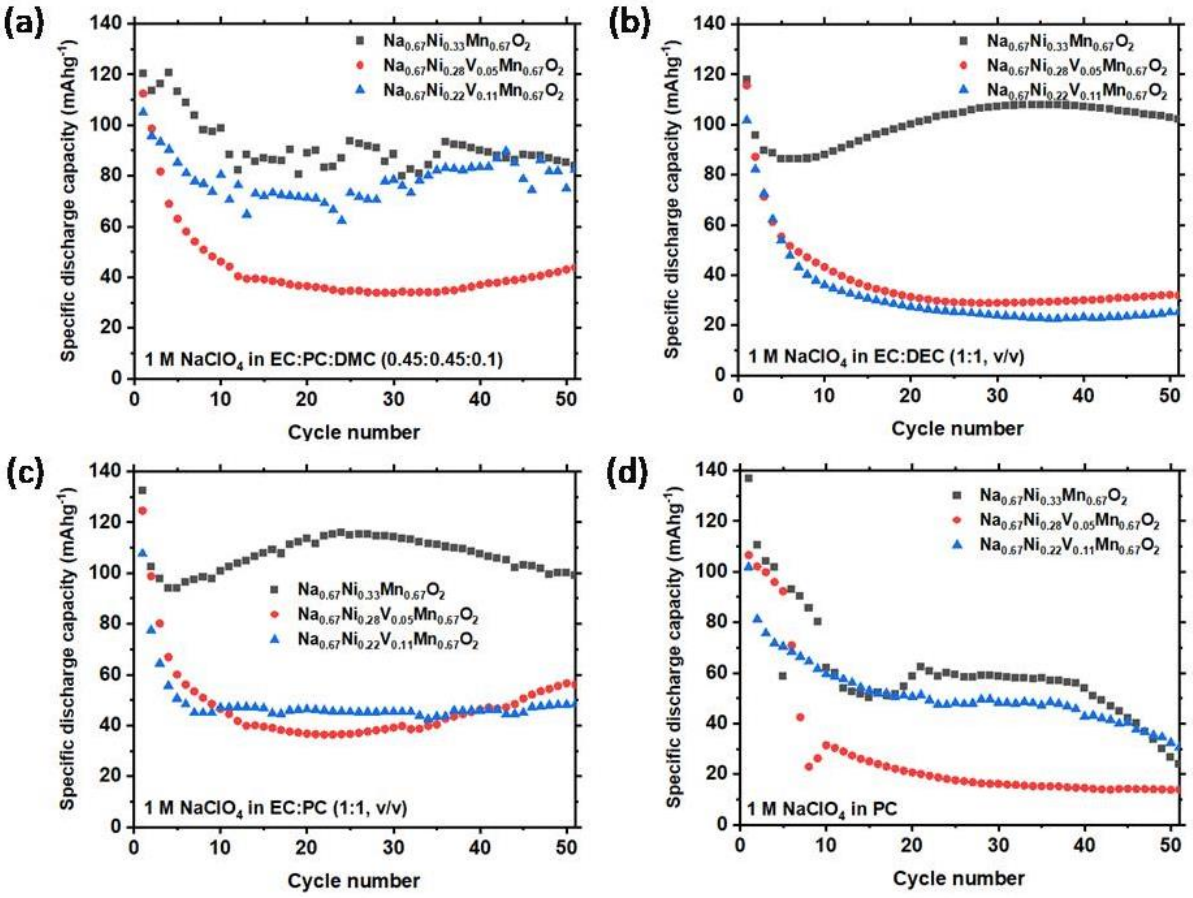

Fig. 9: Cycle stabilities of P2-type $Na_{0.67}Ni_{0.33-x}V_xMn_{0.67}O_2$ samples (where x = 0, 0.05 and 0.11) at the rate of 0.2C between 1.5-4.3 V in various electrolytes (a) 1.0 M $NaClO_4$ in Ethylene carbonate: Propylene carbonate: Dimethyl carbonate (0.45:0.45:0.1), (b) 1.0 M $NaClO_4$ in Ethylene carbonate: Diethyl carbonate (1:1), (c) 1.0 M $NaClO_4$ in Ethylene carbonate: Propylene carbonate (1:1) and (d) 1.0 M $NaClO_4$ in Propylene carbonate.

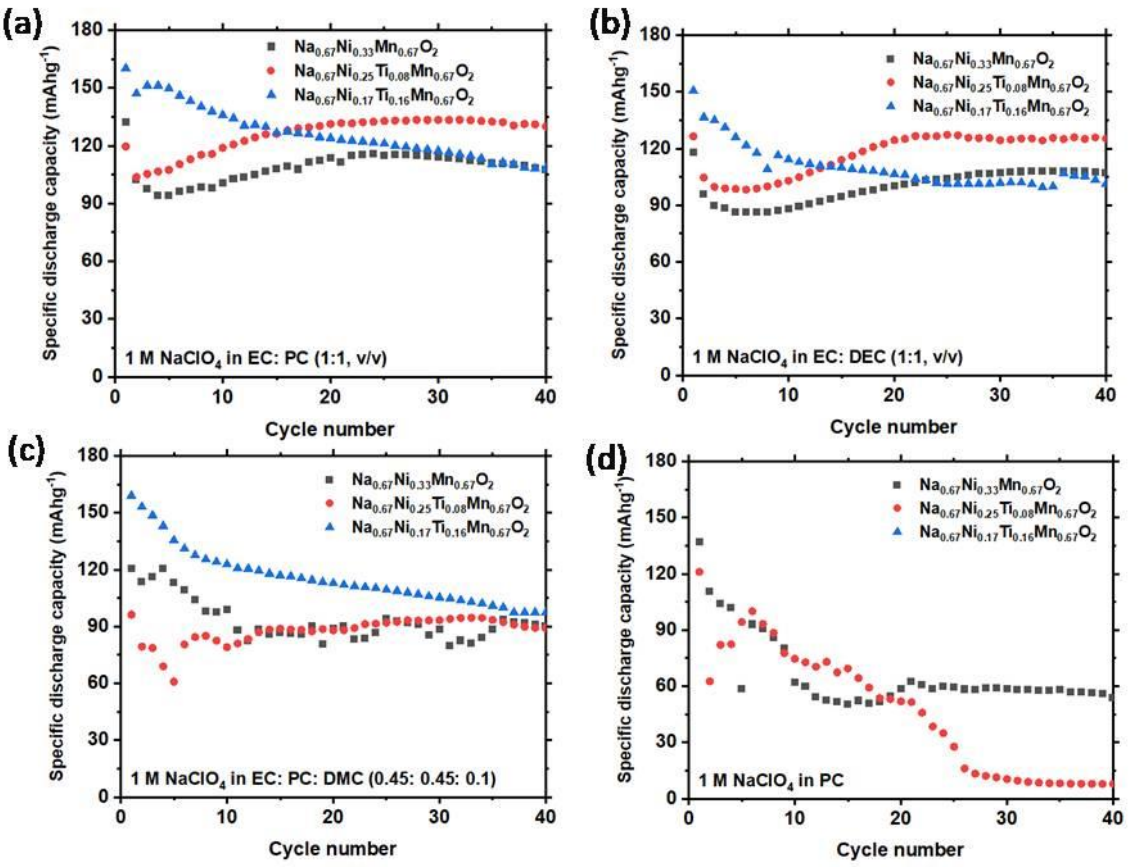

Fig. 10: Cycle stabilities of P2-type $Na_{0.67}Ni_{0.33-x}Ti_xMn_{0.67}O_2$ samples (where x = 0, 0.08 and 0.16) at the rate of 0.2C between 1.5-4.3 V in various electrolytes (a) 1.0 M $NaClO_4$ in Ethylene carbonate: Propylene carbonate (1:1), (b) 1.0 M $NaClO_4$ in Ethylene carbonate: Diethyl carbonate (1:1) and (c) 1.0 M $NaClO_4$ in Ethylene carbonate: Propylene carbonate: Dimethyl carbonate (0.45: 0.45: 0.1).

For a direct comparison, the Ti-substituted P2-type $Na_{0.67}Ni_{0.33-x}Ti_xMn_{0.67}O_2$ electrodes (x = 0, 0.08 and 0.16) were further investigated in three of the above organic ester-based electrolyte systems (EC: PC, EC: DEC and EC: PC: DMC). The cycle stabilities of the electrodes are shown in Fig. 10. Interestingly, both Ti-substituted electrodes exert extended cycle stability as compared to the pristine P2-type $Na_{0.67}Ni_{0.33}Mn_{0.67}O_2$ electrode. $Na_{0.67}Ni_{0.17}Ti_{0.16}Mn_{0.67}O_2$ electrodes offer the highest discharge capacity in all three electrolyte systems. Added contribution from the re-appearance of P2-O2 phase transition and Mn^{3+}/Mn^{4+}-redox reaction counts for the higher capacity of $Na_{0.67}Ni_{0.17}Ti_{0.16}Mn_{0.67}O_2$. The initial discharge capacities of $Na_{0.67}Ni_{0.17}Ti_{0.16}Mn_{0.67}O_2$ electrodes in EC: PC, EC: DEC, and EC: PC: DMC electrolytes were ~160, 151, and 159 $mAhg^{-1,}$ respectively. After 10 charge-discharge cycles, the electrodes have retained 85%, 76%, and 77% of the initial discharge capacities at a rate of 0.2C. The pristine P2-type $Na_{0.67}Ni_{0.33}Mn_{0.67}O_2$ electrode retained 76%, 75%, and 82% of initial discharge capacities at 0.2C. On the other hand, $Na_{0.67}Ni_{0.25}Ti_{0.08}Mn_{0.67}O_2$ cells furnish slightly reduced initial specific capacity of ~120, 127, and 97 $mAhg^{-1}$ in the presence of 1 M $NaClO_4$ in EC: PC, EC: DEC, and EC: PC: DMC electrolytes,

respectively. However, the electrodes extend the best stabilities at a rate of 0.2C, leading to > 95% initial capacity retention in all three electrolyte systems. Meanwhile, both Ti-substituted electrodes perform better capacity retention in longer charge-discharge cycles irrespective of the electrolytic conditions.

4. Conclusion

Phase pure P2-type $Na_{0.67}Ni_{0.33-x}V_xMn_{0.67}O_2$ (x = 0, 0.05 and 0.11) electrode materials have been prepared via facile solid-state synthesis and tested as cathodes for non-aqueous sodium-ion batteries. The material characterization for phase purity, doping concentration, oxidation states of Mn ions was done with X-Ray diffraction, EPR spectroscopy, Raman spectroscopy, and SEM. Aliovalent substitution on Ni- site was done by controlling the Mn^{3+}/Mn^{4+} ratio to improve the electrochemical performance of the sample. In the electrochemical tests, P2-type $Na_{0.67}Ni_{0.28}V_{0.05}Mn_{0.67}O_2$ electrodes serve an initial discharge capacity of 138 $mAhg^{-1}$ in the voltage range 1.5 and 4.1 V. $Na_{0.67}Ni_{0.22}V_{0.11}Mn_{0.67}O_2$ electrodes extended the initial discharge capacity till 146 $mAhg^{-1}$ between 1.5 and 4.1 V. Both V-substituted electrodes lack in providing long cycle stability due to appearance of Jahn-Teller active Mn^{3+}-ions. Ti-substituted P2-type $Na_{0.67}Ni_{0.33-x}Ti_xMn_{0.67}O_2$ electrodes (x = 0, 0.08 and 0.16) offered long cycle stabilities in an earlier study from our group. $Na_{0.67}Ni_{0.25}Ti_{0.08}Mn_{0.67}O_2$ electrodes showed an initial discharge capacity loss of only 12% at the end of the 50 charge-discharge cycles in the upper cut-off voltage of 4.3 V. $Na_{0.67}Ni_{0.17}Ti_{0.16}Mn_{0.67}O_2$/Na half-cells to have displayed exceptionally high cycle stability (81% capacity retention after 120 cycles) in a lower voltage range of 1.5 V–4.1 V. In the present study, capacity retention measurements at a wider voltage range (1.5 V–4.3 V) on P2-type $Na_{0.67}Ni_{0.22}V_{0.11}Mn_{0.67}O_2$ show significant improvement in capacity retention for long cycles. The higher V-substituted $Na_{0.67}Ni_{0.22}V_{0.11}Mn_{0.67}O_2$ electrodes have offered an initial specific discharge capacity of ~155 $mAhg^{-1}$ at a rate of 0.1C. A slow capacity fading is evident with a loss of ~ 24% of the discharge capacity in the initial ten cycles as compared to ~ 50% capacity loss in the pristine compound. P2-type $Na_{0.67}Ni_{0.33-x}V_xMn_{0.67}O_2$ (x = 0, 0.05 and 0.11) electrodes when tested in various organic ester-based electrolyte combinations offer a slight improvement in the capacity retention. $Na_{0.67}Ni_{0.22}V_{0.11}Mn_{0.67}O_2$ electrode retains 79% of its initial capacity in the presence of 1.0 M $NaClO_4$ in EC: PC: DMC (0.45: 0.45: 0.1) electrolyte after 50 charge-discharge cycles. Conversely, Ti-substituted P2-type $Na_{0.67}Ni_{0.33-x}Ti_xMn_{0.67}O_2$ electrodes (x = 0.08 and 0.16) offer significant improvement in the cycle capacity retention. Both of the Ti-substituted electrodes outdo the performances of the parent P2-type $Na_{0.67}Ni_{0.33}Mn_{0.67}O_2$ electrode at the end of the 40^{th} charge-discharge cycle.

References

[1] H. Su, S. Jaffer, H. Yu, Transition metal oxides for sodium-ion batteries, Energy Storage Materials 5 (2016)116–131.

[2] V. Palomares, M. Casas-Cabanas, E. Castillo-Martínez, M. H. Han, T. Rojo, Update on na-based battery materials. A growing research path, Energy & Environmental Science 6 (8) (2013) 2312–2337.

[3] H. Pan, Y.-S. Hu, L. Chen, Room-temperature stationary sodium-ion batteries for large-scale electric energy storage, Energy & Environmental Science 6 (8) (2013) 2338–2360.

[4] S. Wang, C. Sun, N. Wang, Q. Zhang, Ni-and/or Mn-based layered transition metal oxides as cathode materialsfor sodium ion batteries: status, challenges and countermeasures, Journal of Materials Chemistry A 7 (17) (2019)10138–10158.

[5] C. Delmas, C. Fouassier, P. Hagenmuller, Structural classification and properties of the layered oxides, Physica B+C 99 (1-4) (1980) 81–85.

[6] C. Didier, M. Guignard, C. Denage, O. Szajwaj, S. Ito, I. Saadoune, J. Darriet, C. Delmas, Electrochemical Na-deintercalation from $NaVO_2$, Electrochemical and Solid State Letters 14 (5) (2011) A75.

[7] D. Hamani, M. Ati, J.-M. Tarascon, P. Rozier, Na_xVO_2 as possible electrode for Na-ion batteries, Electrochemistry Communications 13 (9) (2011) 938–941.

[8] C. Didier, M. Guignard, J. Darriet, C. Delmas, O3–Na_xVO_2 system: A superstructure for $Na_{1/2}VO_2$, Inorganic Chemistry 51 (20) (2012) 11007–11016.

[9] M. Guignard, C. Didier, J. Darriet, P. Bordet, E. Elkaïm, C. Delmas, P2-Na_xVO_2 system as electrodes for batteries and electron-correlated materials, Nature materials 12 (1) (2013) 74–80.

[10] J. Xu, D. H. Lee, R. J. Clement, X. Yu, M. Leskes, A. J. Pell, G. Pintacuda, X.-Q. Yang, C. P. Grey, Y. S. Meng, Identifying the critical role of li substitution in P2-$N_{ax}[L_{iy}N_{iz}M_{n1-y-z}]O2$ (0<x, y, z<1) intercalation cathode materials for high-energy na-ion batteries, Chemistry of Materials 26 (2) (2014) 1260–1269.

[11] P.-F. Wang, Y. You, Y.-X. Yin, Y.-S. Wang, L.-J. Wan, L. Gu, Y.-G. Guo, Suppressing the P2-O2 phase transition of $Na_{0.67}Mn_{0.67}Ni_{0.33}O_2$ by magnesium substitution for improved sodium-ion batteries, Angewandte Chemie 128 (26) (2016) 7571–7575.

[12] X. Wu, J. Guo, D. Wang, G. Zhong, M. J. McDonald, Y. Yang, P2-type $Na_{0.67}Ni_{0.33-x}Zn_xMn_{0.67}O_2$ as new high-voltage cathode materials for sodium-ion batteries, Journal of Power Sources 281 (2015) 18–26.

[13] K. Kubota, Y. Yoda, S. Komaba, Origin of enhanced capacity retention of P2-type $Na_{2/3}Ni_{1/3-x}Cu_xMn_{2/3}O_2$ for Na-ion batteries, Journal of The Electrochemical Society 164 (12) (2017) A2368.

[14] D. Yuan, X. Hu, J. Qian, F. Pei, F. Wu, R. Mao, X. Ai, H. Yang, Y. Cao, P2-type $Na_{0.67}Mn_{0.65}Fe_{0.2}Ni_{0.15}O_2$ cathode material with high-capacity for sodium-ion battery, Electrochimica Acta 116 (2014) 300–305.

[15] Z.-Y. Li, J. Zhang, R. Gao, H. Zhang, Z. Hu, X. Liu, Unveiling the role of co in improving the high-rate capability and cycling performance of layered $Na_{0.7}Mn_{0.7}Ni_{0.3-x}Co_xO_2$ cathode materials for sodium-ion batteries, ACS applied materials & interfaces 8 (24) (2016) 15439–15448.

[16] W. Zhao, A. Tanaka, K. Momosaki, S. Yamamoto, F. Zhang, Q. Guo, H. Noguchi, Enhanced electrochemical performance of Ti substituted P2-$Na_{2/3}Ni_{1/4}Mn_{3/4}O_2$ cathode material for sodium ion batteries, Electrochimica Acta 170 (2015) 171–181.

[17] Chagas, L. G., Buchholz, D., Vaalma, C., Wu, L., & Passerini, S. (2014). P-type Na x Ni 0.22 Co 0.11 Mn 0.66 O 2 materials: linking synthesis with structure and electrochemical performance. Journal of Materials Chemistry A, 2(47), 20263-20270.

[18] Kataoka, R., Mukai, T., Yoshizawa, A., Inoue, K., Kiyobayashi, T., & Sakai, T. (2015). High capacity positive electrode material for room temperature Na ion battery: NaxMn2/3Co1/6Ni1/6O2. Journal of The Electrochemical Society, 162(4), A553.

[19] Zheng, L., Li, J., & Obrovac, M. N. (2017). Crystal structures and electrochemical performance of air-stable

Na2/3Ni1/3–x Cu x Mn2/3O2 in sodium cells. Chemistry of Materials, 29(4), 1623-1631.
[20] D. Pahari, S. Puravankara, On controlling the P2-O2 phase transition by optimal Ti-substitution on Ni-site in P2-type $Na_{0.67}Ni_{0.33}Mn_{0.67}O_2$ (NNMO) cathode for Na-ion batteries, Journal of Power Sources 455 (2020) 227957.
[21] Kim, D., Lee, E., Slater, M., Lu, W., Rood, S., & Johnson, C. S. (2012). Layered Na [Ni1/3Fe1/3Mn1/3] O2 cathodes for Na-ion battery application. Electrochemistry Communications, 18, 66-69.
[22] Yoshida, H., Yabuuchi, N., Kubota, K., Ikeuchi, I., Garsuch, A., Schulz-Dobrick, M., & Komaba, S. (2014). P2-type Na 2/3 Ni 1/3 Mn 2/3− x Ti x O 2 as a new positive electrode for higher energy Na-ion batteries. Chemical communications, 50(28), 3677-3680.
[23] C.Bommier, X. Ji, Electrolytes, SEI Formation, and Binders: A Review of Nonelectrode Factors for Sodium-Ion Battery Anodes. Small (2018) 14(16) 1703576.
[24] Ponrouch, A., Marchante, E., Courty, M., Tarascon, J. M., & Palacín, M. R. (2012). In search of an optimized electrolyte for Na-ion batteries. Energy & Environmental Science, 5(9), 8572-8583.
[25] Sun, Y., Shi, P., Xiang, H., Liang, X., & Yu, Y. (2019). High-Safety Nonaqueous Electrolytes and Interphases for Sodium-Ion Batteries. Small, 15(14), 1805479.
[26] Li, Q., Chen, J., Fan, L., Kong, X., & Lu, Y. (2016). Progress in electrolytes for rechargeable Li-based batteries and beyond. Green Energy & Environment, 1(1), 18-42.
[27] Ponrouch, A., Dedryvère, R., Monti, D., Demet, A. E., Mba, J. M. A., Croguennec, L., ... & Palacín, M. R. (2013). Towards high energy density sodium ion batteries through electrolyte optimization. Energy & Environmental Science, 6(8), 2361-2369.
[28] Z. Lu, J. Dahn, In situ x-ray diffraction study of P2-$Na_{2/3}Ni_{1/3}Mn_{2/3}O_2$, Journal of the Electrochemical Society 148 (11) (2001) A1225.
[29] H. Che, S. Chen, Y. Xie, H. Wang, K. Amine, X.-Z. Liao, Z.-F. Ma, Electrolyte design strategies and research progress for room-temperature sodium-ion batteries, Energy & Environmental Science 10 (5) (2017) 1075–1101.
[30] Y. Liu, X. Fang, A. Zhang, C. Shen, Q. Liu, H. A. Enaya, C. Zhou, Layered P2-$Na_{2/3}[Ni_{1/3}Mn_{2/3}]O_2$ as high-voltage cathode for sodium-ion batteries: the capacity decay mechanism and Al_2O_3 surface modification, Nano Energy 27 (2016) 27–34.
[31] H. Wang, B. Yang, X.-Z. Liao, J. Xu, D. Yang, Y.-S. He, Z.-F. Ma, Electrochemical properties of P2-$Na_{2/3}[Ni_{1/3}Mn_{2/3}]O_2$ cathode material for sodium ion batteries when cycled in different voltage ranges, Electrochimica Acta 113 (2013) 200–204.
[32] S. Y. Lee, J. H. Kim, Y. C. Kang, Electrochemical properties of P2-type $Na_{2/3}Ni_{1/3}Mn_{2/3}O_2$ plates synthesized by spray pyrolysis process for sodium-ion batteries, Electrochimica Acta 225 (2017) 86–92.
[33] A. Ponrouch, D. Monti, A. Boschin, B. Steen, P. Johansson, M. R. Palacín, Non-aqueous electrolytes for sodium-ion batteries, Journal of Materials Chemistry A 3 (1) (2015) 22–42.
[34] R. Stoyanova, E. Zhecheva, S. Vassilev, Mn^{4+} environment in layered $Li[Mg_{0.5-x}Ni_xMn_{0.5}]O_2$ oxides monitoredby epr spectroscopy, Journal of Solid State Chemistry 179 (2) (2006) 378–388.
[35] G. Singh, J. M. L. del Amo, M. Galceran, S. Perez-Villar, T. Rojo, Structural evolution during sodium de-intercalation/intercalation in $Na_{2/3}[Fe_{1/2}Mn_{1/2}]O_2$, Journal of Materials Chemistry A 3 (13) (2015) 6954–6961.
[36] Wang, H., Yang, B., Liao, X. Z., Xu, J., Yang, D., He, Y. S., & Ma, Z. F. (2013). Electrochemical properties of P2-$Na_{2/3}[Ni_{1/3}Mn_{2/3}]O_2$ cathode material for sodium ion batteries when cycled in different voltage ranges. Electrochimica Acta, 113, 200-204.
[37] Gutierrez, A., Dose, W. M., Borkiewicz, O., Guo, F., Avdeev, M., Kim, S., ... & Johnson, C. S. (2018). On disrupting the Na^+-ion/vacancy ordering in P2-type sodium–manganese–nickel oxide cathodes for Na^+-ion batteries. The Journal of Physical Chemistry C, 122(41), 23251-23260.
[38] Manikandan, P., Ramasubramonian, D., & Shaijumon, M. M. (2016). Layered P2-type $Na_{0.5}Ni_{0.25}Mn_{0.75}O_2$ as a high performance cathode material for sodium-ion batteries. Electrochimica Acta, 206, 199-206.

[39] N. Yabuuchi, M. Kajiyama, J. Iwatate, H. Nishikawa, S. Hitomi, R. Okuyama, R. Usui, Y. Yamada and S. Komaba, Nat. Mater., 2012, 11, 512–516.
[40] Talaie, E., Duffort, V., Smith, H. L., Fultz, B., & Nazar, L. F. (2015). Structure of the high voltage phase of layered P2-Na 2/3− z [Mn 1/2 Fe 1/2] O 2 and the positive effect of Ni substitution on its stability. Energy & Environmental Science, 8(8), 2512-2523.
[41] Biecher, Y., Smiley, D. L., Guignard, M., Fauth, F., Berthelot, R., Delmas, C., ... & Carlier, D. (2020). Original Layered OP4-(Li, Na) x CoO2 Phase: Insights on Its Structure, Electronic Structure, and Dynamics from Solid State NMR. Inorganic chemistry, 59(8), 5339-5349.
[42] Clement, R. J., Billaud, J., Armstrong, A. R., Singh, G., Rojo, T., Bruce, P. G., & Grey, C. P. (2016). Structurally stable Mg-doped P2-Na 2/3 Mn 1− y Mg y O 2 sodium-ion battery cathodes with high rate performance: insights from electrochemical, NMR and diffraction studies. Energy & Environmental Science, 9(10), 3240-3251.
[43] Somerville, J. W., Sobkowiak, A., Tapia-Ruiz, N., Billaud, J., Lozano, J. G., House, R. A., ... & Bruce, P. G. (2019). Nature of the "Z"-phase in layered Na-ion battery cathodes. Energy & Environmental Science, 12(7), 2223-2232.
[44] Li, Y., Yang, Z., Xu, S., Mu, L., Gu, L., Hu, Y. S., ... & Chen, L. (2015). Air-Stable Copper-Based P2-$Na_{7/9}Cu_{2/9}Fe_{1/9}Mn_{2/3}O_2$ as a New Positive Electrode Material for Sodium-Ion Batteries. Advanced Science, 2(6), 1500031.
[45] Billaud, J., Singh, G., Armstrong, A. R., Gonzalo, E., Roddatis, V., Armand, M., ... & Bruce, P. G. (2014). Na 0.67 Mn 1− x Mg x O 2 (0≤ x≤ 0.2): a high capacity cathode for sodium-ion batteries. Energy & Environmental Science, 7(4), 1387-1391.
[46] Clement, R. J., Bruce, P. G., & Grey, C. P. (2015). manganese-based P2-type transition metal oxides as sodium-ion battery cathode materials. Journal of The Electrochemical Society, 162(14), A2589.
[47] Komaba, S., Murata, W., Ishikawa, T., Yabuuchi, N., Ozeki, T., Nakayama, T., ... & Fujiwara, K. (2011). Electrochemical Na insertion and solid electrolyte interphase for hard-carbon electrodes and application to Na-Ion batteries. Advanced Functional Materials, 21(20), 3859-3867.
[48] Ponrouch, A., Goñi, A. R., & Palacin, M. R. (2013). High capacity hard carbon anodes for sodium ion batteries in additive free electrolyte. Electrochemistry communications, 27, 85-88.
[49] Wang, L., Huang, K. W., Chen, J., & Zheng, J. (2019). Ultralong cycle stability of aqueous zinc-ion batteries with zinc vanadium oxide cathodes. Science advances, 5(10), eaax4279.
[50] Schon, T. B., An, S. Y., Tilley, A. J., & Seferos, D. S. (2019). Unusual capacity increases with cycling for ladder-type microporous polymers. ACS applied materials & interfaces, 11(2), 1739-1747.

Supporting Information

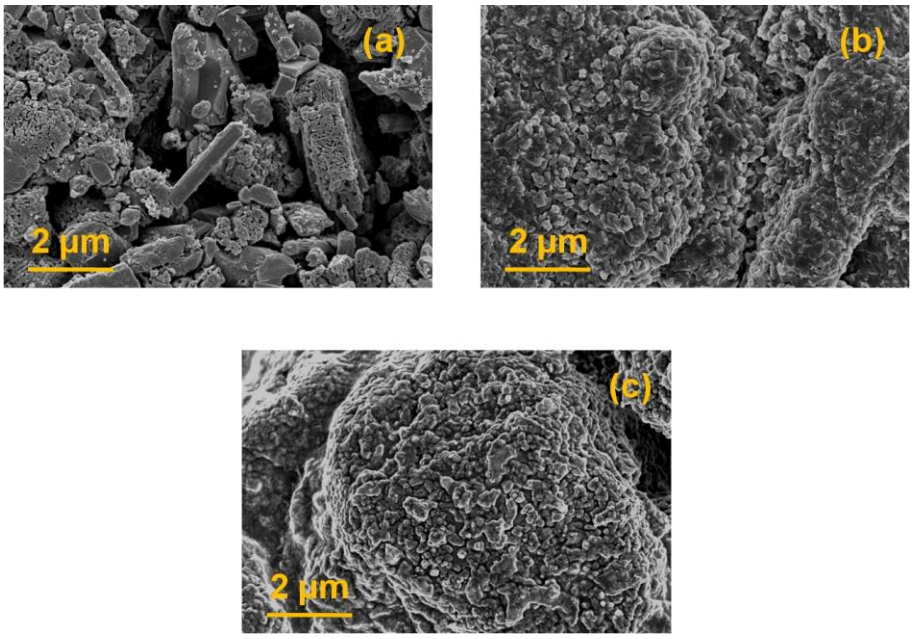

Fig. SI 1: SEM images of P2-type $Na_{0.67}Ni_{0.33-x}V_xMn_{0.67}O_2$ [x = 0 (a), 0.05 (b) and 0.11(c)] samples.

(a)

Element	Weight%	Atomic%
Mn K	67.07	68.52
Ni K	32.93	31.48
Totals	100.00	

(b)

Element	Weight%	Atomic%
V K	6.13	6.70
Mn K	65.26	66.15
Ni K	28.62	27.15
Totals	100.00	

(c)

Element	Weight%	Atomic%
V K	13.64	14.77
Mn K	62.90	63.18
Ni K	23.46	22.05
Totals	100.00	

Fig. SI 2: *Energy-dispersive* X-ray spectroscopy (EDX) analysis of P2-$Na_{0.67}Ni_{0.33-x}V_xMn_{0.67}O_2$ [x = 0 (a), 0.05 (b) and 0.11 (c)] samples.

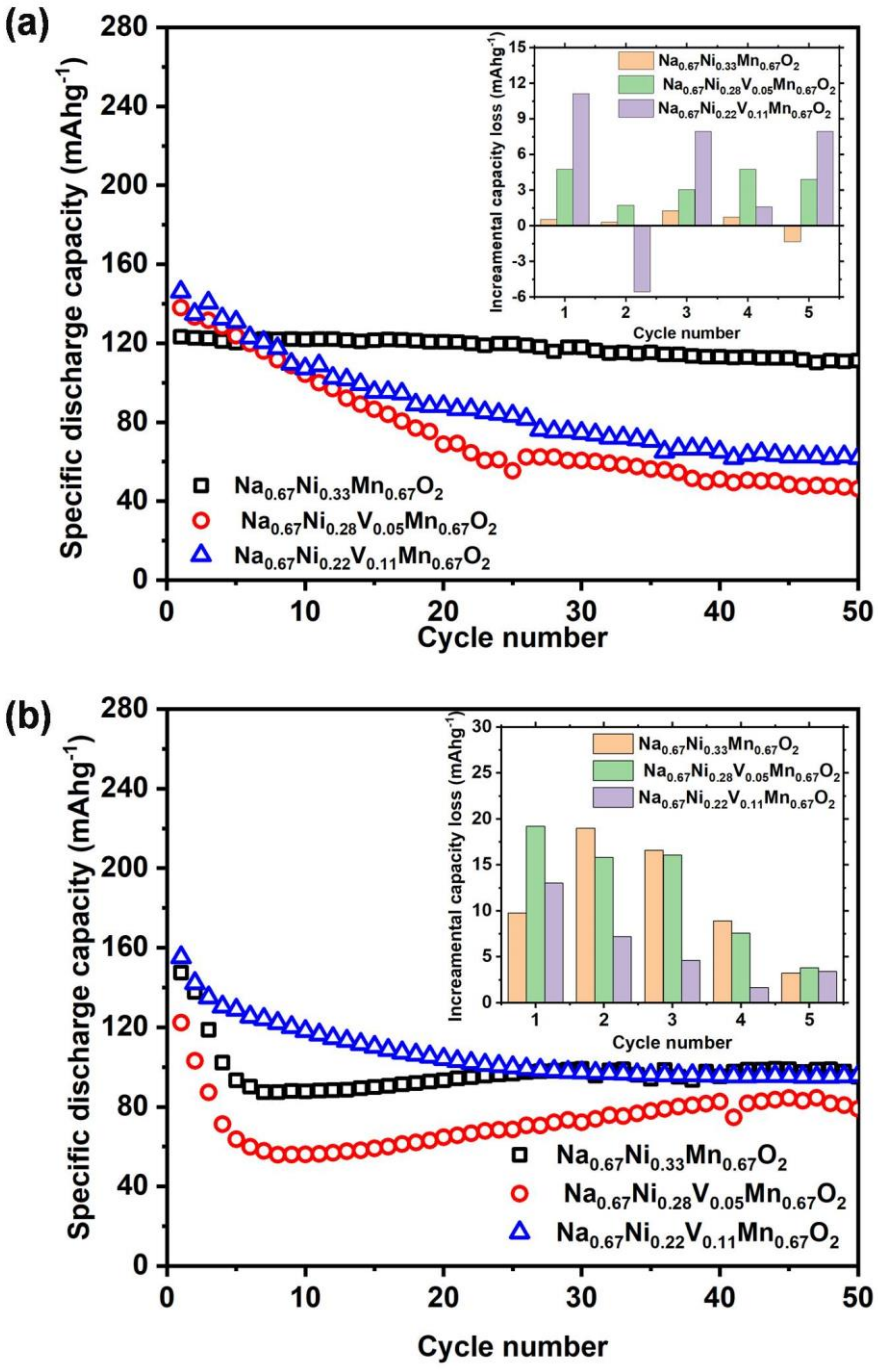

Fig. SI 3: Cycle stabilities of P2-type $Na_{0.67}Ni_{0.33-x}V_xMn_{0.67}O_2$ samples (where x= 0, 0.05 and 0.11) (a) at the rate of 0.05 C between 1.5- 4.1 V and (b) at the rate of 0.1 C between 1.5- 4.3 V. The incremental capacity losses for first 5 cycles have been depicted in insets.

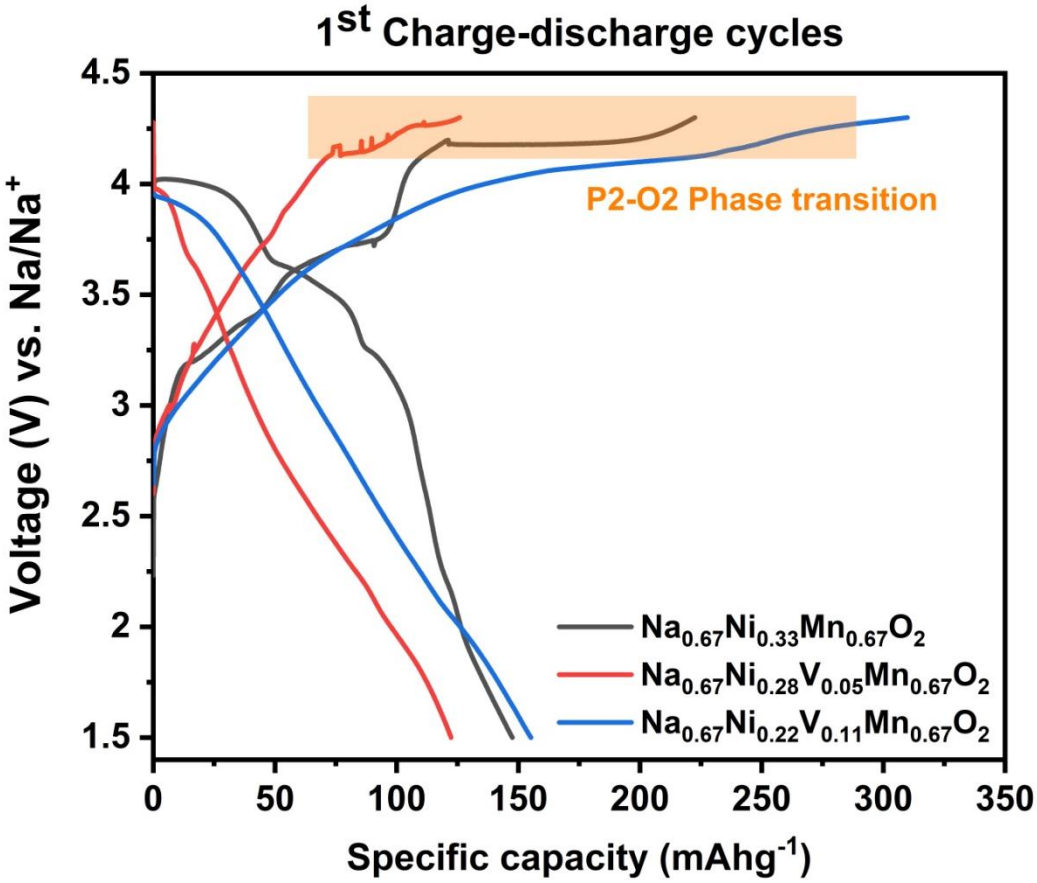

Fig. SI 4: First charge-discharge cycles of P2-type $Na_{0.67}Ni_{0.33-x}V_xMn_{0.67}O_2$ samples (where x= 0, 0.05 and 0.11) at the rate of 0.1 C between 1.5- 4.3 V.